PRELIMINARY RESULTS ON THE FRACTURE ANALYSIS OF MULTI-SITE CRACKING OF LAP JOINTS IN AIRCRAFT SKINS

J. L. Beuth, Jr. and J. W. Hutchinson
Division of Applied Sciences, Harvard University
Cambridge, MA 02138

INTRODUCTION

This paper presents results of a fracture mechanics analysis relevant to fatigue crack growth at rivets in lap joints of aircraft skins. Multi-site damage (MSD) is receiving increased attention within the context of problems of aging aircraft. Fracture analyses carried out previously include small-scale modeling of rivet/skin interactions, larger-scale two-dimensional models of lap joints similar to that developed here, and full scale three-dimensional models of large portions of the aircraft fuselage. Fatigue testing efforts have included flat coupon specimens, two-dimensional lap joint tests, and full scale tests on specimens designed to closely duplicate aircraft sections. Most of this work is documented in the proceedings of previous symposia on the aging aircraft problem. Other sources include reference 1, which provides a detailed summary of final results from the testing and finite element analysis of full-scale models of aircraft sections. References 2 and 3 offer analyses of the interaction of large-scale aircraft skin cracks with stiffeners in the absence of MSD. The effect MSD has on the ability of skin stiffeners to arrest the growth of long skin cracks is a particularly important topic that remains to be addressed.

One of the most striking features of MSD observed in joints of some test sections and in the joints of some of the older aircraft fuselages is the relative uniformity of the fatigue cracks from rivet to rivet along an extended row of rivets. This regularity suggests that nucleation of the cracks must not be overly difficult. Moreover, it indicates that there is some mechanism which keeps longer cracks from running away from shorter ones, or, equivalently, a mechanism for shorter cracks to "catch-up" with longer cracks. This basic mechanism has not been identified, and one of the objectives of the present work is to see to what extent the mechanism is revealed by a fracture analysis of the MSD cracks. Another related aim is to present accurate stress intensity factor variations with crack length which can be used to estimate fatigue crack growth lifetimes once cracks have been initiated. Results will be presented which illustrate the influence of load shedding from rivets with long cracks to neighboring rivets with shorter cracks. Results will also be included for the effect of residual stress due to the riveting process itself. All the results presented in this paper should be regarded as preliminary in the sense that further work by ourselves and

C-2

others will be required to validate them and to establish their sensitivity to more embellished modelling assumptions.

MODEL

The model is defined with reference to figures 1 and 2. The joint is imagined to be infinite in width with three rows of rivets equally spaced a distance 2w apart in the x-direction. The vertical spacing between the rows is h, and the rivet radius is R. The average stress carried across the joint is Σ_{yy}. As indicated in figure 1, a straight crack of length a emerges from the horizontal extremity of each side of each rivet hole in the top row of the outside skin. Each section of width 2w containing a line of 3 rivets deforms identically, and thus attention can be directed to the behavior of just one section, such as that in figure 1. Furthermore, each section is symmetric with respect to the plane x=0, so that only one half of a section needs to be modelled, as shown in figure 2. Periodic boundary conditions must be enforced on the right vertical edges of the model. These require that the shear stress vanishes along the edges, and that the edges remain straight and parallel to the y-axis. The average strain in the x-direction (the relative horizontal displacement of the edges divided by 2w) must be such that the stress in the skin well away from the joint is Σ_{xx}. In this preliminary study, finite element calculations were made with $\Sigma_{xx}=0$; however, the effects of nonzero transverse loading are approximated using a solution in the literature.

Bending out of the plane will be neglected. Each half of the lapped skin is modeled by a thin plate, or sheet, in plane stress with load transferred from one to the other through rivets which are modeled in a manner discussed below. Three-dimensional aspects of the rivet geometry, such as countersinking, are ignored. Residual stress in the rivet and skin in the vicinity of the rivet hole due to the riveting process is likely to effect fatigue crack growth, and an initial attempt to assess this effect is included in a subsequent section of the paper. Bonding by an adhesive layer between the lapped sheets is not considered. Plasticity is not taken into account; deformations are assumed to be elastic. Some of the effects being ignored are likely to be important, and it is our intention to include them in a more elaborate model in the near future.

The next section presents stress concentration factors for the uncracked joint after several ways to model the rivet/skin interaction have been discussed. The sections following then present stress intensity factors for the MSD cracks, an approximate analysis of the role of residual stress induced by the riveting process, and preliminary work related to load shedding from rivets with longer cracks to rivets with shorter cracks. The calculations reported below have been carried out using dimensions of a typical aircraft lap joint with w=0.50 in., h=1.00 in., R=0.0805 in., and d=0.50 in. Thus, the nondimensional ratios used in the calculations are

$$h / R = 12.42, \quad w / R = 6.21, \quad d / R = 6.21 \tag{1}$$

The material properties used for aircraft skin were E=10.0 Msi and ν=1/3.

STRESS CONCENTRATION AT THE RIVET HOLES IN THE ABSENCE OF CRACKS

A finite element model of the section shown in figure 2 has been developed using the ABAQUS code with eight-noded quadrilateral plane stress elements. Details of the rivet/sheet interaction will be shown to be very important. In the present study two simplified models of rivet/sheet interaction are used, in each case with rivets taken to be rigid with zero friction where they contact the boundary of the rivet hole. Thus, for both models, the displacements of the rivet center points A, B, and C for the outside skin (figure 2) were set equal, respectively, to those of rivet center points A', B', and C' for the inside skin. Some of the additional details of this modelling are described below. The effect of more elaborate modelling assumptions will be explored in subsequent work.

The problem of a rigid rivet contacting a rivet hole is, in general, nonlinear requiring iteration of some kind to determine the contact region. In this paper two models of the interaction will be pursued which we believe are limiting cases of the full range of behavior. One of the modelling assumptions is appropriate when there is little or no residual stress exerted by the rivet on the unloaded sheet so that the rivet separates from the hole when the joint is loaded (BC#1), and the other applies when the residual stress due to the riveting process results in the maintenance of contact between rivet and sheet around the entire circumference of the hole (BC#2). In the first case, in which the rivet is assumed to just fit into its hole with no residual stress acting across the hole boundary, exploratory calculations showed that under application of Σ_{yy} only the bottom half of the rivets contacted the holes of the outside sheet (and the top half of the rivets for the inside sheet), with the exception in a few cases where a very small contact zone existed just above the crack line in the outside sheet. Thus, for all the results presented in this section and the next section for the case BC#1, the contact region was assumed a priori to coincide with the lower half of the rivets for the outside sheet and the upper half of the rivets for the inside sheet. This boundary condition, together with the condition that the shear traction vanish over the contacting regions, is conveniently incorporated in the ABAQUS code. For the case in which residual stress forces contact over the entire circumference of the hole, the boundary condition is modified accordingly, retaining the assumption that shear tractions vanish everywhere around the hole. The effect of the residual stress distribution itself on the stress intensity factor of the crack will be taken up in the next section.

The mesh used when no cracks are present (a=0) is shown in figure 3a. Care was taken to ensure that the computed stress concentration factors (SCFs) did not change with further refinement of the mesh. In the absence of the cracks, the behavior of the top and bottom sheets is identical and this was exploited to mesh just the outside sheet. In this single sheet model, the vertical displacement of point B is set equal to zero and the displacements of points A and C are constrained to be equal in magnitude and opposite in sign. The calculations for the SCFs, and for the stress intensity factors in the next section, were made with zero average transverse stress, i.e. $\Sigma_{xx}=0$. In a pressurized fuselage, a reasonable approximation for Σ_{xx} would be $\Sigma_{yy}/2$, but many tests are carried out with $\Sigma_{xx}=0$. In the next section, a simple approximation for including the influence of the transverse stress will be suggested.

With σ_{yy} as the stress component at the edge of the hole, directly to the left or right of its center, let $SCF = \sigma_{yy}/\Sigma_{yy}$. The SCFs at the holes in the outside sheet calculated using the rigid rivet model for the case BC#1 are

$$SCF_{\text{top hole}} = 4.43, \qquad SCF_{\text{middle hole}} = 2.79, \qquad SCF_{\text{bottom hole}} = 2.72 \tag{2}$$

The larger value at the top hole relative to the lower holes in the top sheet mainly reflects the fact the average of the stress component σ_{yy} carried by the top sheet is significantly higher above the top row of rivets than below it due to load transfer to the inside sheet. To examine the possible effect of rivet stiffness in shear, another calculation which takes the shear load carried by each of the three rivets to be the same (as would be expected in the extreme limit of very compliant rivets) has been carried out. It gives the following rather similar results

$$SCF_{\text{top hole}} = 4.25, \qquad SCF_{\text{middle hole}} = 3.28, \qquad SCF_{\text{bottom hole}} = 2.39 \tag{3}$$

Three-dimensional effects (e.g. countersinking and elasticity of the rivets) will effect local stress concentration factors in the vicinity of the holes before any cracks develop. The absolute values of the SCFs presented above are therefore not expected to be of particular significance. However, the relative levels do clearly indicate that fatigue cracks would be expected to start at the top hole of the outside sheet or at the bottom hole of the inside sheet, assuming that some additional factor such as countersinking did not differentiate between the two sheets.

ENERGY RELEASE RATE, STRESS INTENSITY FACTORS, AND COMPLIANCE CHANGE DUE TO CRACKING

As depicted in figure 2, cracks of length a are assumed to exist in the top sheet, emerging on each side of the top rivet hole at its horizontal extremities. The cracks are taken to be straight

and parallel to the x-axis. The energy release rate, $\mathcal{G}$, the mode I and II stress intensity factors, K_I and K_{II}, and the compliance change due to the presence of the cracks have been calculated as a function of the crack length for the case of no transverse loading, $\Sigma_{xx}=0$ for each of the two rivet/sheet boundary conditions.

Figures 3b and 3c give close-ups of the top portion of the outside sheet with the near-tip finite element mesh inserted. Both sheets must be meshed for the crack problem since only the outside sheet contains the cracks, and the problem is no longer symmetric with respect to the two sheets. Refinements of the near-tip mesh have been made for 9 distinct crack lengths. The elements nearest to the tip are composed of quarter-point elements to model the inverse square root singularity of the stresses and strains. The radial length of the smallest elements ranged from $6.13 \times 10^{-4}R$ for a crack of length a/R=0.199 to $3.69 \times 10^{-3}R$ for a crack of length a/R=3.61. The energy release rate, $\mathcal{G}$, was calculated using the J-integral option in ABAQUS. Let $\psi=\tan^{-1}(K_{II}/K_I)$ be the measure of the relative proportion of mode II to mode I. The values of ψ were computed using values of the tangential and opening components of the crack face displacements behind the tip. The distance behind the tip used for this evaluation was chosen to be that where the independent evaluation of $\mathcal{G}$ from the crack opening displacements gave the best agreement with the more accurate J-integral estimate of $\mathcal{G}$. The values of ψ are not expected to be as accurate as those for $\mathcal{G}$, but the crack tip is so nearly in a state of pure mode I that this is not a significant consideration.

Define a measure of the magnitude of the stress intensity factors by

$$K = \sqrt{EG} = \sqrt{K_I^2 + K_{II}^2} \tag{4}$$

where the last equality follows from the plane stress relation $\mathcal{G}=(K_I^2+K_{II}^2)/E$. With these definitions

$$K_I = K\cos\psi \quad \text{and} \quad K_{II} = K\sin\psi \tag{5}$$

The curves of $K/(\Sigma_{yy}\sqrt{R})$ versus a/R for the two rivet conditions are shown in figure 4, and values are recorded in table 1. These results were computed using the nondimensional lengths in equation (1). The corresponding curves of ψ as a function of a/R are given in figure 5. For each of the two rivet boundary conditions the magnitude of ψ is small; to an extremely good approximation the crack is a mode I crack with $K_I=K$. However ψ is negative for BC#1 implying that there is a tendency for the crack to curve upward slightly, while for BC#2 the trend would be for the crack to curve downward.

There is no hint of an explanation of the "catch-up" phenomenon in the results of K versus a, although K is only a weakly increasing function of the range of a/R for each of the two cases. If the functional relationship had displayed a local peak for crack lengths on the order of the rivet radius or so, then that feature might help to explain how shorter cracks could

grow faster than somewhat longer cracks and thus tend to catch-up in length. A local peak had seemed a plausible possibility because of the high stress concentration at the edge of the hole, but it does not exist according to either of the present models. It must be remembered that the residual stress contribution to the stress intensity factor has not yet been included in the lower curve in figure 4 for BC#2, and its inclusion can lead to a broad local peak as will be seen in the next section. First, however, an approximate way to include the effect of the transverse loading, Σ_{xx}, on K will be given.

The problem of a traction-free hole with symmetric edge cracks in an infinite sheet has been solved in the literature (refs. 4 and 5) for the case where the remote stress is Σ_{xx}. The result can be written as

$$\frac{K}{\Sigma_{xx}\sqrt{R}} = -\sqrt{\pi\frac{a}{R}}F(s), \qquad s = \frac{a}{R+a} \tag{6}$$

where F(s) is given in the Appendix. For crack lengths which are large compared to R, this result is clearly a poor approximation because of the interaction of the cracks with the edges of the section. However, the main influence of this contribution is for relatively short cracks. This is evident in figure 4 where K for the case of no residual stress (BC#1) is given by the superposition of the previous result for $\Sigma_{xx}=0$ and equation (6) with $\Sigma_{xx}=\Sigma_{yy}/2$, corresponding to the proportion of loads for a pressurized cylindrical shell. The influence of the transverse contribution is relatively small over the entire range of a/R. The accuracy of the simple approximation in equation (6), which neglects any interaction with the rivet, can be readily checked by calculations using the present model. This will be done in future work. Given the small influence of the transverse component of loading on the result in figure 4, it is not expected that more accurate modeling will change conclusions drawn based on calculations carried out with $\Sigma_{xx}=0$.

The compliance change due to the presence of the MSD cracks can be computed using the well known relationship between the derivative of compliance with respect to crack length and the energy release rate, or it can be determined directly from the finite element results. As a check on the computations, both determinations were carried out and found to be in agreement.

THE ROLE OF RESIDUAL STRESSES AT THE RIVET HOLES

For BC#2 it has been assumed that the rivets maintain contact with the holes in the sheets due to residual stress induced in the riveting process. However, the results in figure 4 for this case do not include any effect of the residual stress other than the consequence of full contact. In this section, an approximate analysis of the residual stress contribution to K will be given. Any contribution to the stress intensity factor due to residual stress at a rivet hole is not cyclic but remains steady as Σ_{yy} and Σ_{xx} undergo cycles of loading and unloading. In this section, we wish

to distinguish between contributions to K from the residual stress which does not cycle and those from the remote loads which do. For this purpose, now let Σ_{yy} and Σ_{xx} be the *peak* values of the remote loads which are assumed to cycle between zero values and these peak values. Let ΔK denote the cyclic change in K associated with the cyclically applied remote loads, as obtained using the results given in the previous section for BC#2. The estimate for the non-cyclic contribution to K from the residual stress is then used in combination with ΔK to calculate the variation of K_{max} and K_{min} as a function of a/R where $K_{min}=K_{residual\ stress}$ and $K_{max}=K_{residual\ stress}+\Delta K$.

An estimate of the stress intensity factor is obtained in the Appendix for cracks emerging from a rivet hole where there is a pre-existing residual stress field due to the riveting process. The model applies to an isolated rivet in an infinite sheet (see the insert in figure 6) and assumes that the radial mismatch strain between the rivet and the hole is ε^T. The elasticity of the rivet is neglected, and the radial stress exerted by the rivet on the *uncracked* sheet at r=R is $\sigma_R=E\varepsilon^T/(1+\nu)$. The stress intensity factor at the tip of the emerging crack with radius a has the form

$$\frac{K}{\sigma_R\sqrt{R}}=\sqrt{\pi\frac{a}{R}}G\left(\frac{a}{R}\right) \tag{7}$$

This relation is plotted in figure 6.

Curves of the normalized K_{max} are plotted as a function of a/R in figure 7 for various values of the ratio of the residual stress to the cyclically applied remote stress, σ_R/Σ_{yy}. Here, the transverse loading, Σ_{xx}, has been taken to be zero, but its effect is not expected to be large, as previously discussed. Companion curves for K_{min} are readily generated using the results in figure 6. If one assumes that the riveting process induces some plastic yielding in the sheet, then a reasonable estimate for σ_R should fall between $\sigma_Y/2$ and σ_Y, where σ_Y is the tensile yield stress of the sheet material. Based on typical values of σ_Y and Σ_{yy} for commercial aircraft, the range of σ_R/Σ_{yy} is expected to fall in the range 1.5 to about 3. The curve of normalized K_{max} versus a/R is flat over much of the range of a/R of interest when $\sigma_R/\Sigma_{yy}=2$ and actually has a broad peak with its maximum occurring at $a/R\cong 0.5$ when $\sigma_R/\Sigma_{yy}=3$. Any conclusions concerning implications for the "catch-up" phenomenon must also take into account the trends for K_{min} and the dependence of the fatigue crack growth rates on both of the parameters characterizing the stress intensity factor cyclic history. Work along these lines will follow in a subsequent paper.

Another feature of the results in figure 7 is that for values of the residual stress parameter σ_R/Σ_{yy} in the range from 2 to 3 the values of K_{max} are not very different from those which would be predicted for the model with BC#1 in figure 4. When a/R is larger than about 3 the K-values for BC#1 reflect the strong interaction between neighboring cracks. This interaction is somewhat

suppressed by the full contact condition which is assumed for the rivet for BC#2. When the cracks become long, the full contact condition is almost certainly unrealistic and separation of the rivet and sheet is expected at the top of the loading cycle. In other words, we believe that BC#1 more realistically models the rivet/sheet interaction even in the presence of residual stress when the cracks become sufficiently long. The present results for the two cases give a clear indication of the range of the stress intensity factor variations which can be expected. It remains to more completely analyze the problem in order to ascertain when one or the other of modeling conditions are appropriate and whether other more detailed models need to be considered.

LOAD SHEDDING

Another explanation of "catch-up" which seems plausible is connected with load shedding. The load shedding idea suggests that if one crack is longer than its neighbor, it will shed some of the load its section carries to the section of its neighbor, thereby increasing the level of the shorter crack's stress intensity factor and providing a means for the shorter crack to grow faster. By considering alternating long and short cracks of length a_1 and a_2, as indicated in figure 8, one can develop a model along the lines of that described in the previous two sections except that now the periodic section is twice as wide. The section used in carrying out the finite element calculations is shown in figure 8. Precisely the same element meshes used in the earlier sections were used here, but these were now linked together to provide meshes appropriate for the two differing crack lengths. Table 2 lists the stress intensity factors calculated for the unequal crack lengths for the case of rivet conditions BC#1. Included in this table are the stress intensity factors for each of the crack lengths as calculated in the previous section where all cracks are of equal lengths. The differences between the stress intensity factors for a crack of given length in the two calculations is less than 1 percent. One concludes from this that, for cracks with $a/R < 1.5$, there is almost no crack interaction and negligible load shedding.

CONCLUSIONS

Basic results have been presented for stress intensity factors for MSD cracks. These results bring out the sensitivity of the predictions to the assumptions made in modeling the rivet/skin interaction. Further work, both theoretical and experimental, needs to be carried out to better characterize this interaction. The results for the two modeling assumptions made in this paper are not substantially different when the residual stress contributions to the stress intensity factors are taken into account. Nevertheless, these predictions should be regarded as preliminary subject to validation by further study. In addition, no effort has been made to include effects due to out-of-plane bending, plasticity, or three dimensionality. One or more of these effects may be

important in MSD cracking. Finally, no dramatic indicator of a catch-up mechanism has emerged in the present work, although the predicted stress intensity factor variation with crack length is relatively weak, especially for the case involving residual stress, suggesting that long and short cracks would grow at roughly the same rate.

ACKNOWLEDGEMENT

This work was supported in part by the Federal Aviation Administration through support from the Transportation Systems Center of the Department of Transportation, in part by the National Science Foundation (Grant MSM-88-12779) and by the Division of Applied Sciences, Harvard University.

REFERENCES

1. Samavedam, G. and Hoadley, D., "Fracture and Fatigue Strength Evaluation of Multiple Site Damaged Aircraft Fuselages - Curved Panel Testing and Analysis," U.S. Department of Transportation Technical Report, March, 1991.

2. Tong, P., "A Hybrid Finite Element Method for Damage Tolerance Analysis," *Computers and Structures*, Vol. 19, No. 1-2, 1984, pp. 263-269.

3. Swift, T., "Important Considerations in Commercial Aircraft Damage Tolerance," *Int. J. of Vehicle Design,* Vol. 7, No. 3-4, 1986, pp. 264-287.

4. Newman, J. C., Jr., *An Improved Method of Collocation for the Stress Analysis of Cracked Plates with Various Shaped Boundaries,* NASA Technical Note, NASA TN D-6376, August, 1971.

5. Tada, H., Paris, P. and Irwin, G., *The Stress Analysis of Cracks Handbook*, 2nd Edn., Paris Productions, Inc., St. Louis, 1985.

APPENDIX

Stress Intensity Factor due to Transverse Loading

The result in equation 6 for the transverse loading Σ_{xx} with $\Sigma_{yy}=0$ has been taken from reference 5. The expression for F(s) is

$$F(s) = 0.5(3-s)\left[1+1.243(1-s)^3\right]-1-(1-s)\left[0.5+0.743(1-s)^2\right] \qquad \text{(A1)}$$

Stress Intensity Factor due to Residual Stress at the Rivet Hole

This is an approximate result which is developed using the solution for the stress intensity factor given in reference 5 for the problem of a hole of radius R with cracks of length a emanating from its horizontal extremities, where the surface of the hole (but not the crack faces) is subject to a uniform pressure, p. That solution is $K=p(\pi a)^{1/2}H(s)$ where $s=a/(R+a)$ and

$$H(s) = (1-s)\left[0.637 + 0.485(1-s)^2 + 0.4s^2(1-s)\right] \tag{A2}$$

The approximate solution will also make use of the *additional* average outward radial displacement at the hole surface δ due to the presence of the two edge cracks of length a. This quantity can be derived from the relation between δ and the energy release rate

$$G = -\frac{1}{2}\left(\frac{\partial(\text{Potential Energy})}{\partial a}\right)_p = \frac{\pi}{2}Rp\frac{\partial\delta}{\partial a} \tag{A3}$$

The result is $\delta=(2pR/E)f_\delta(a/R)$ where

$$f_\delta\left(\frac{a}{R}\right) = \int_0^{a/R} H(s)^2 \frac{a}{R}\frac{da}{R} \tag{A4}$$

The radial displacement of the hole without cracks present when subject to a pressure p is $u=pR(1+\nu)/E$. If it is assumed that there is a strain misfit between the rivet and the hole, ε^T, and that the rivet is effectively rigid, then an approximate condition for determining p as a function of the length of the cracks is $u+\delta=R\varepsilon^T$. This equation gives

$$p = \sigma_R\left[1+\left(\frac{2}{1+\nu}\right)f_\delta\left(\frac{a}{R}\right)\right]^{-1} \quad \text{where} \quad \sigma_R = \frac{E\varepsilon^T}{1+\nu} \tag{A5}$$

Note that σ_R is the normal stress exerted by the rivet on the hole when a=0. This result in combination with equation A2 gives the desired result, equation 7, where

$$G\left(\frac{a}{R}\right) = H(s)\left[1+\left(\frac{2}{1+\nu}\right)f_\delta\left(\frac{a}{R}\right)\right]^{-1} \tag{A6}$$

Table 1

Normalized Stress Intensity Factors $K_{norm}=\frac{K}{\Sigma_{yy}\sqrt{R}}$ for

Two Sets of Rivet/Skin Boundary Conditions ($\Sigma_{xx}=0$)

a/R	Knorm for BC#1	Knorm for BC#2
0.199	2.440	0.502
0.371	2.723	0.656
0.586	2.906	0.799
0.855	3.072	0.948
1.192	3.268	1.109
1.612	3.530	1.291
2.137	3.899	1.502
2.794	4.479	1.763
3.615	5.557	2.125

Table 2

Results for the Load Shedding Analysis

Using BC#1 Rivet/Skin Interaction Conditions ($\Sigma_{xx}=0$)

a/R for Crack 1	a/R for Crack 2	Knorm for Crack 1	Knorm for Crack 2
0.586	0.586	2.906	2.906
0.855	0.586	3.069	2.908
0.855	0.855	3.072	3.072
1.192	0.855	3.265	3.075
1.192	1.192	3.268	3.268

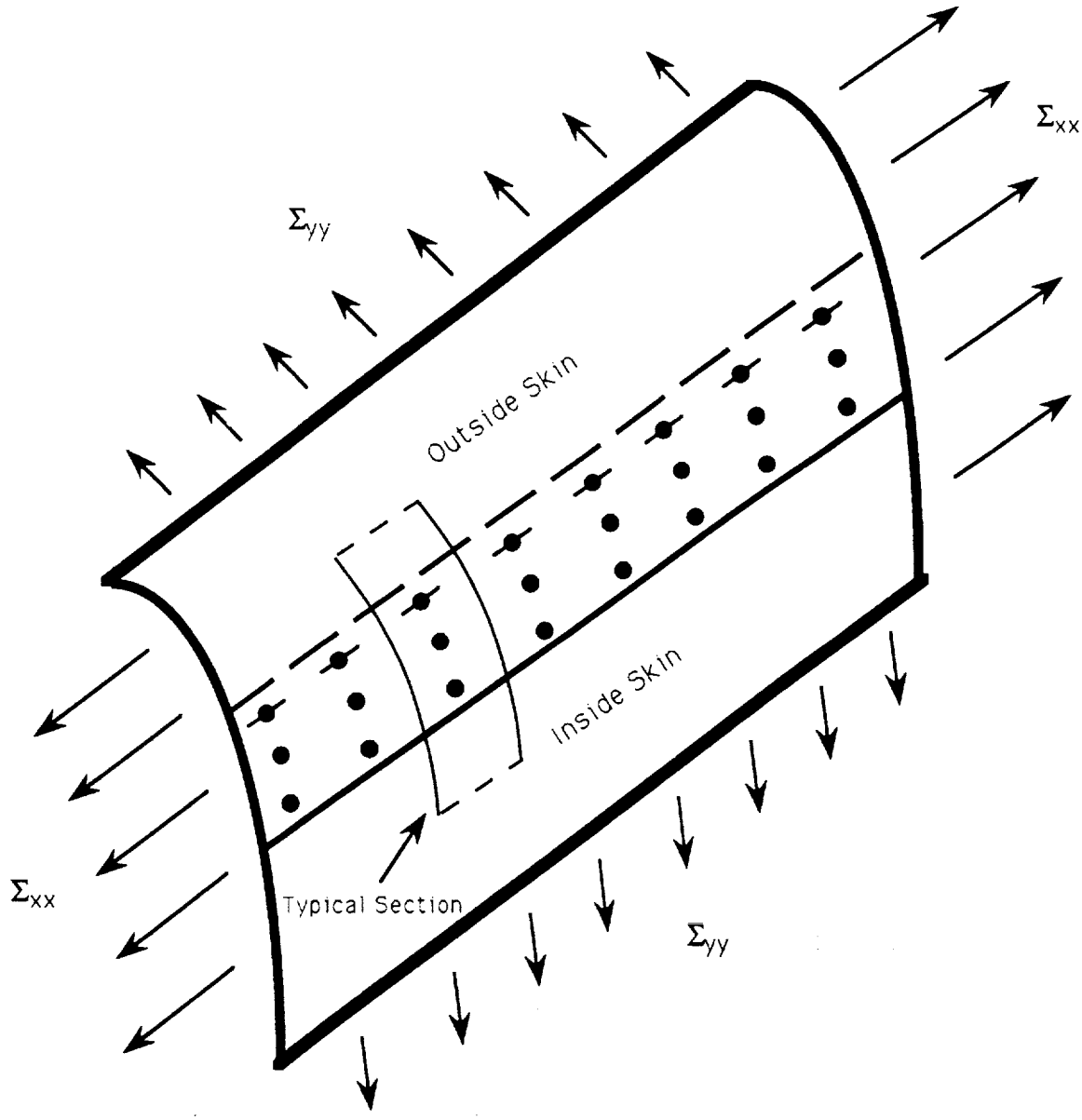

Figure 1 Geometry and loading of the lap joint.

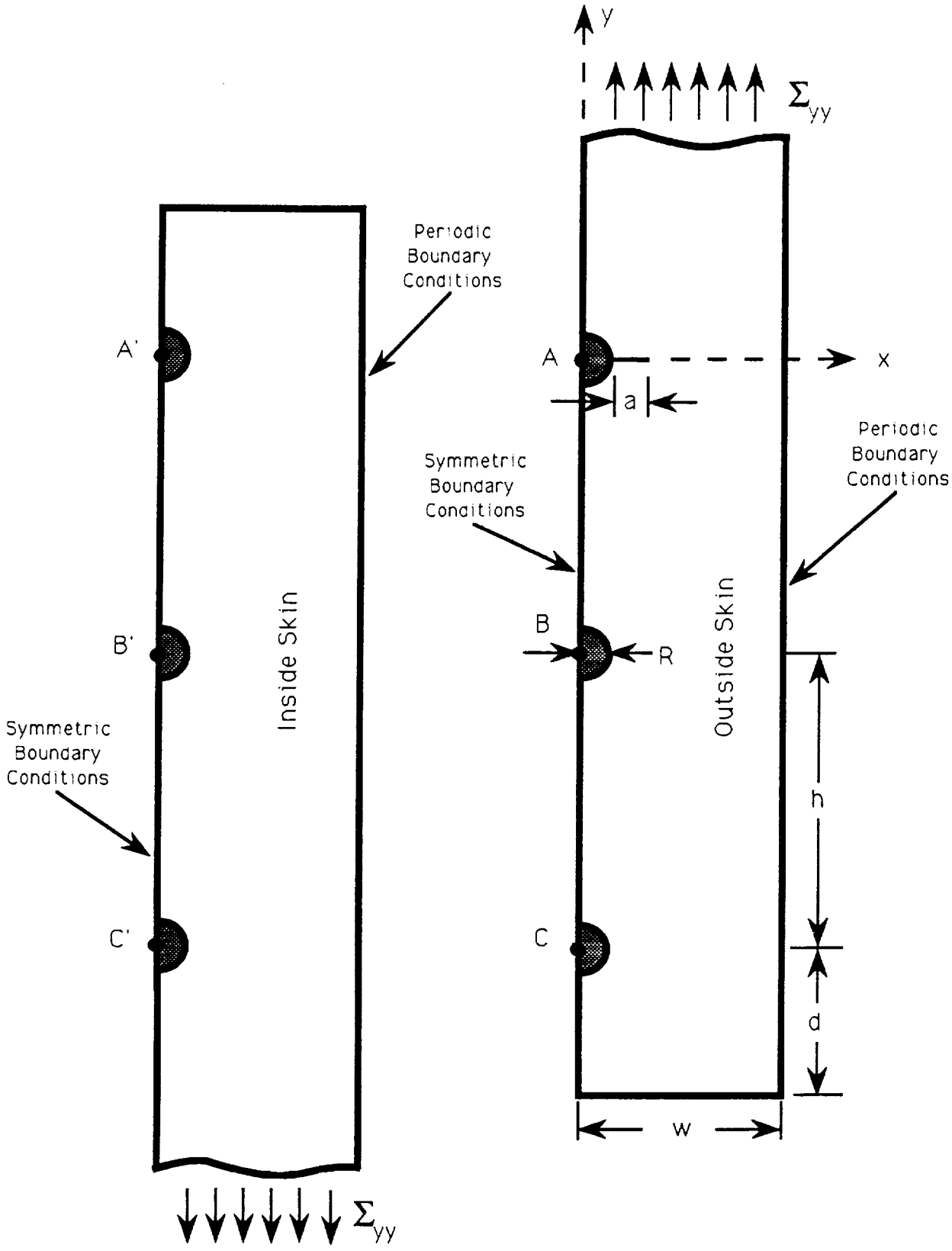

Figure 2 Sections used in the finite element model with $\Sigma_{xx}=0$.

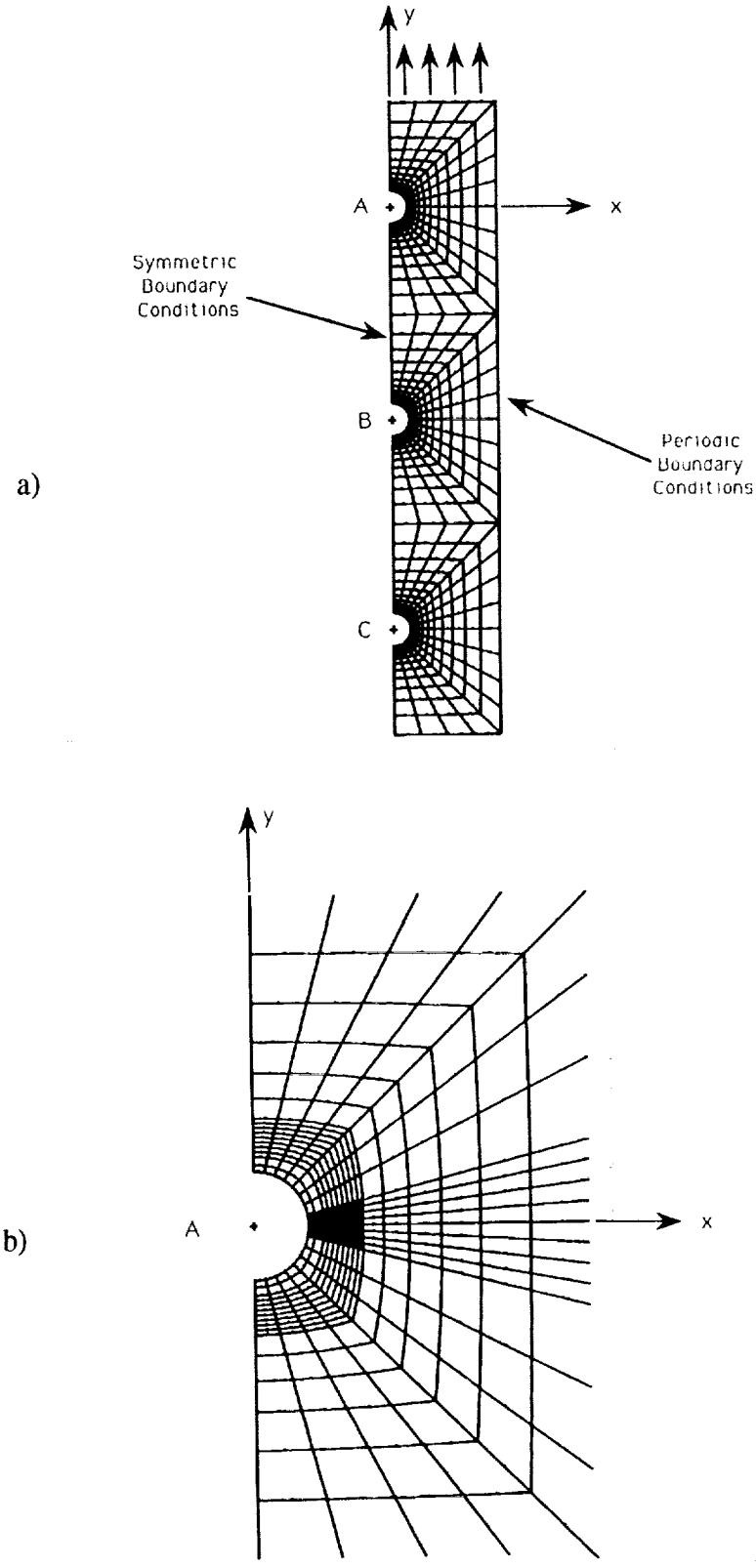

Figure 3 a) Finite element mesh for section without cracks. b) Local mesh near the cracked rivet hole.

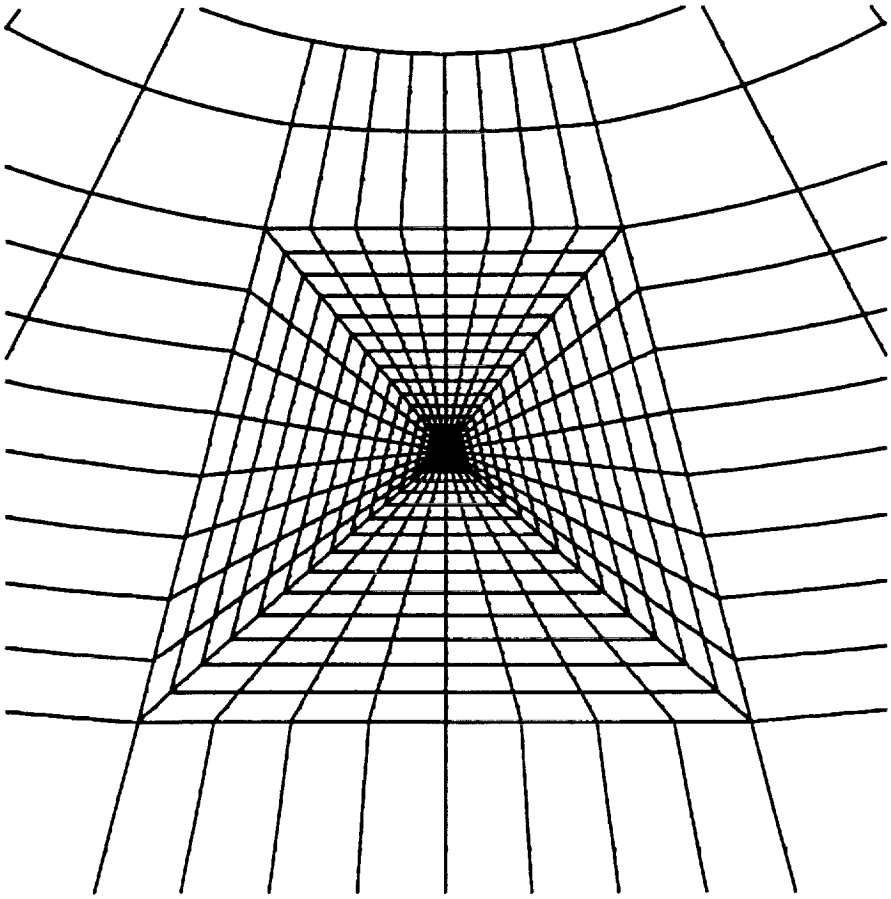

Figure 3c) Close-up of local mesh near the cracked rivet hole.

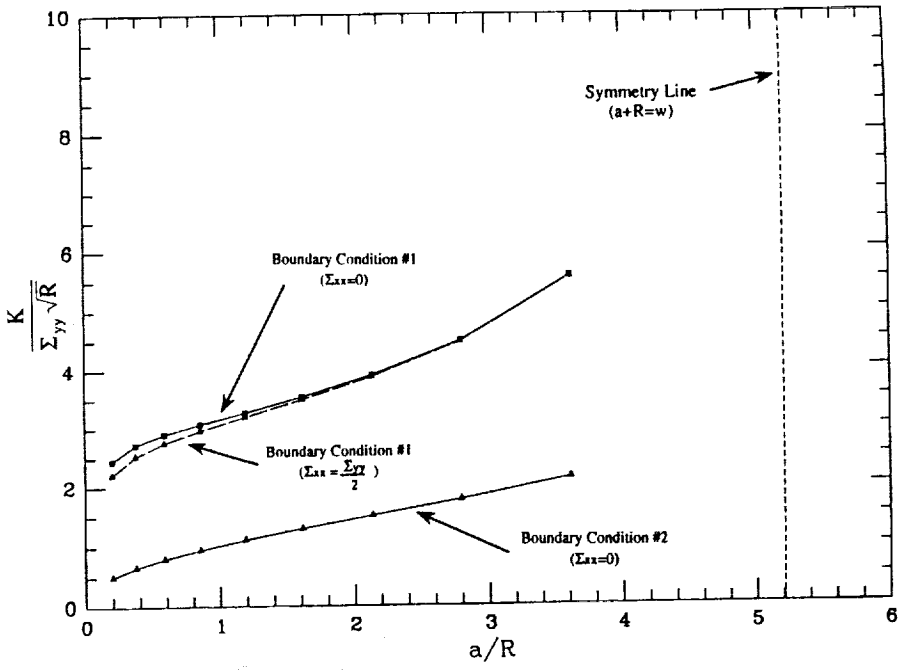

Figure 4 Normalized stress intensity factors as a function of normalized crack length for the two sets of rivet/skin boundary conditions.

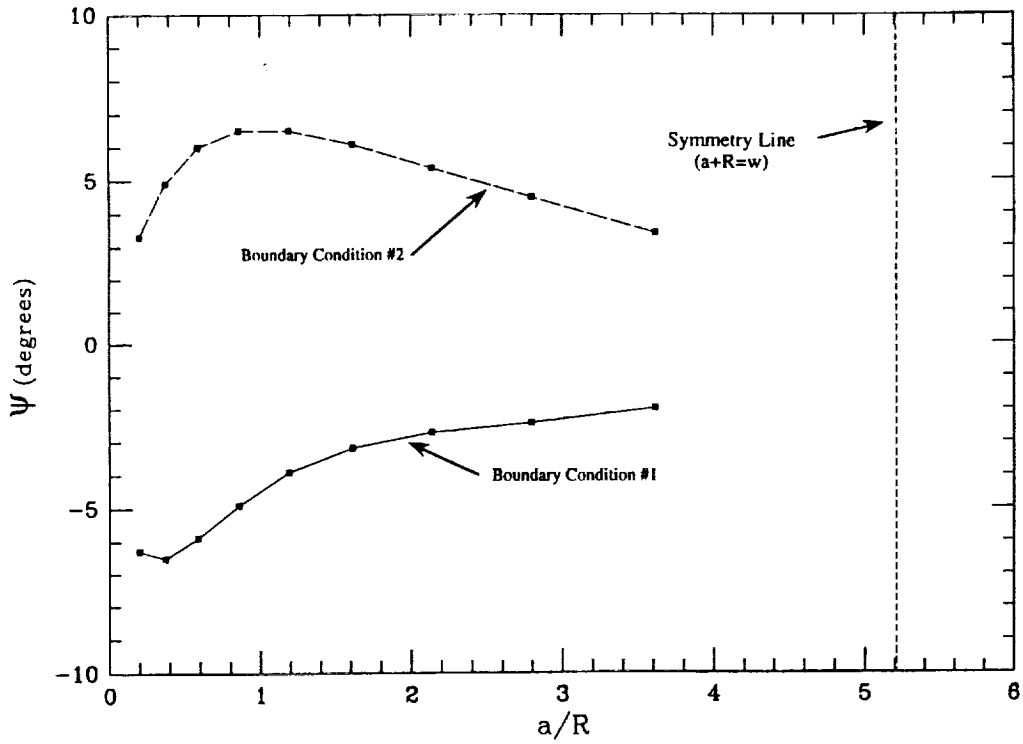

Figure 5 Measure of mode mixity at the crack tip for two sets of boundary conditions.

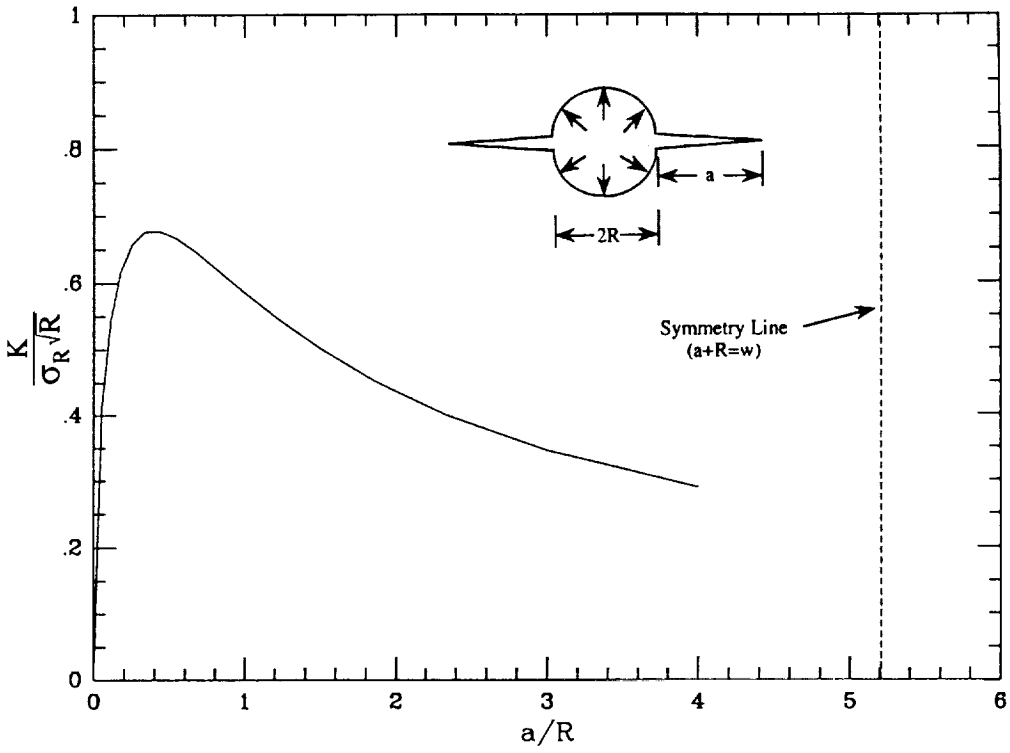

Figure 6 Normalized stress intensity factor contribution due to residual stress.

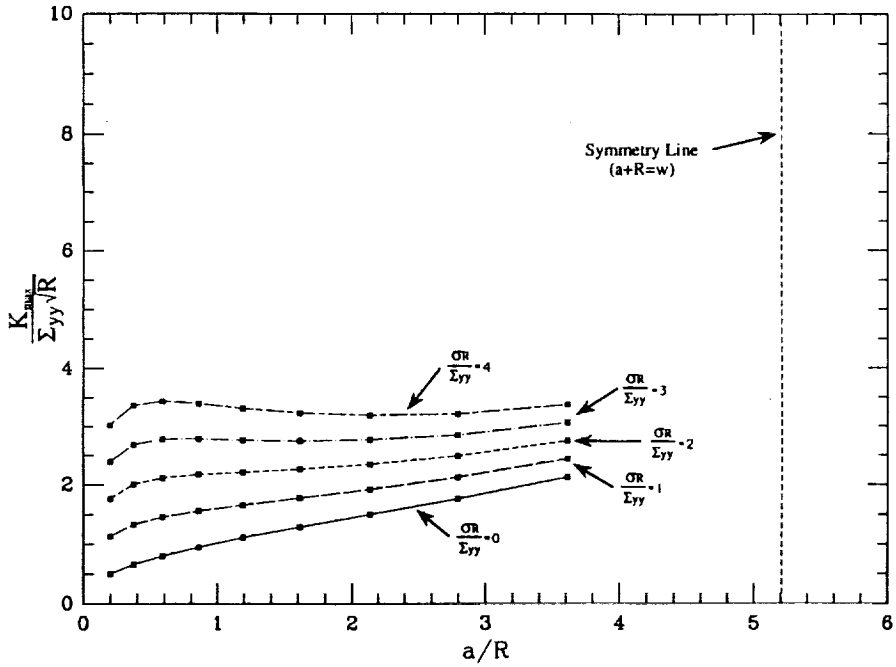

Figure 7 Normalized maximum stress intensity factors for Boundary Condition #2, including the effect of residual stress.

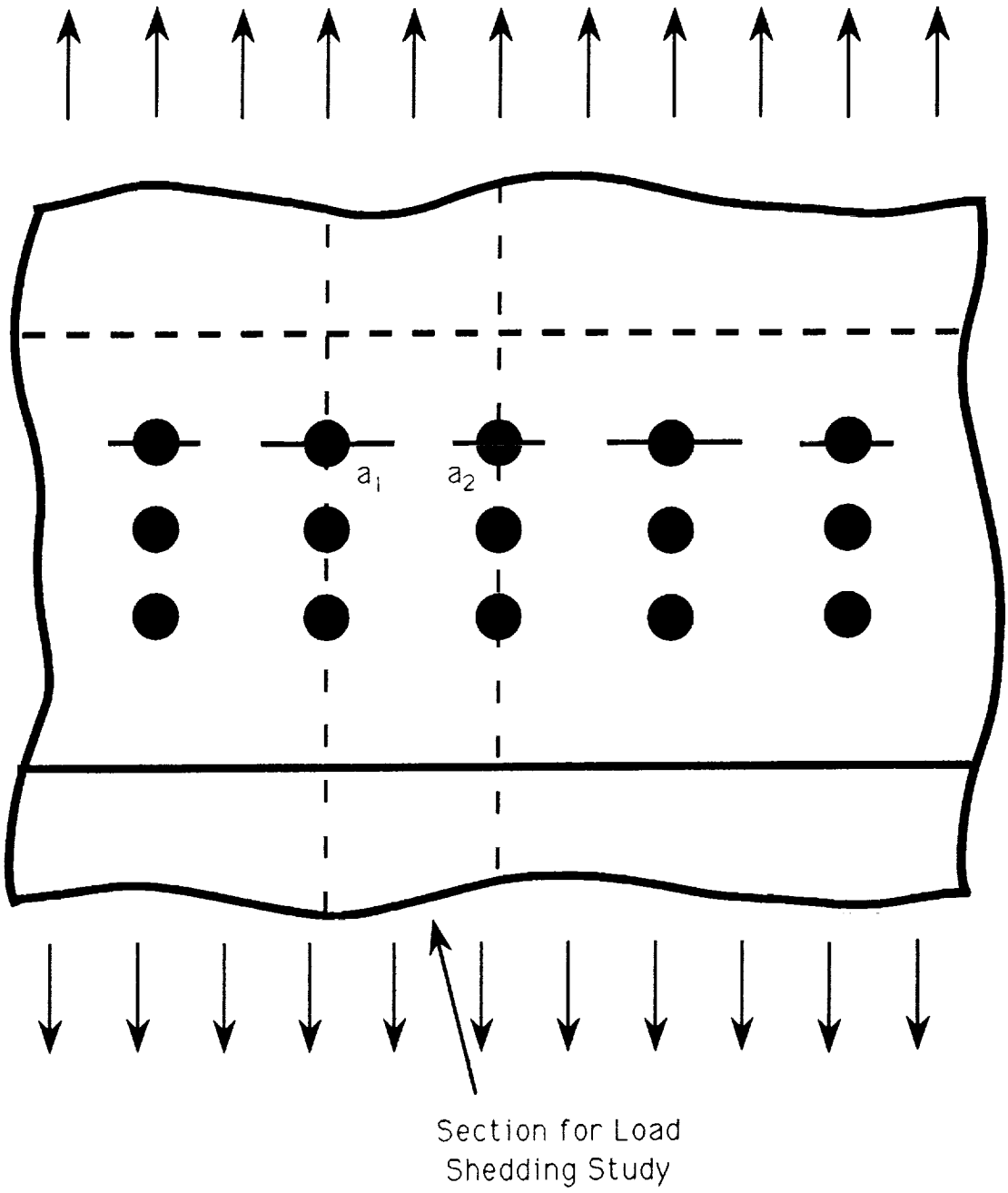

Figure 8 Geometry for the load shedding study.